Biophysical Journal
Article

Biophysical Society

Single-virus content-mixing assay reveals cholesterol-enhanced influenza membrane fusion efficiency

Katherine N. Liu[1] and Steven G. Boxer[1,*]
[1]Department of Chemistry, Stanford University, Stanford, California

ABSTRACT To infect a cell, enveloped viruses must first undergo membrane fusion, which proceeds through a hemifusion intermediate, followed by the formation of a fusion pore through which the viral genome is transferred to a target cell. Single-virus fusion studies to elucidate the dynamics of content mixing typically require extensive fluorescent labeling of viral contents. The labeling process must be optimized depending on the virus identity and strain and can potentially be perturbative to viral fusion behavior. Here, we introduce a single-virus assay in which content-labeled vesicles are bound to unlabeled influenza A virus (IAV) to eliminate the problematic step of content-labeling virions. We use fluorescence microscopy to observe individual, pH-triggered content mixing and content-loss events between IAV and target vesicles of varying cholesterol compositions. We show that target membrane cholesterol increases the efficiency of IAV content mixing and decreases the fraction of content-mixing events that result in content loss. These results are consistent with previous findings that cholesterol stabilizes pore formation in IAV entry and limits leakage after pore formation. We also show that content loss due to hemagglutinin fusion peptide engagement with the target membrane is independent of composition. This approach is a promising strategy for studying the single-virus content-mixing kinetics of other enveloped viruses.

SIGNIFICANCE To replicate, enveloped viruses, like influenza A virus, must successfully deliver their contents to a host cell through viral membrane fusion. Most single-virus fusion assays require extensive fluorescent labeling of virions, which can be perturbative to fusion kinetics. Here, we utilize content-labeled vesicles in a single-virus content-mixing assay, which eliminates the need to fluorescently label virus contents. We use this assay to show that target membrane cholesterol increases the fraction of stable influenza virus content-mixing events. This assay also enables the study of target membrane destabilization because of viral fusion peptide engagement.

INTRODUCTION

The transfer of genetic information from a virus to a host cell is a critical precursor for viral replication. For enveloped viruses, in order for this transfer to occur, the viral membrane must fuse to a host membrane, which is followed by the formation of a fusion pore through which the viral genome is transferred into the target cell (1,2). For viruses that have segmented genomes, like influenza A virus (IAV), effective genome transfer is especially vital to produce replicated virions that are fully functional.

IAV entry occurs in the endosome and is mediated by its envelope protein hemagglutinin (HA). Fusion is triggered by low pH as the endosome matures, and HA undergoes a large conformational rearrangement to insert its hydrophobic fusion peptide into the host membrane (3,4). Kinetic studies and simulations have shown that for IAV fusion to occur, several neighboring HA fusion peptides must successfully engage with the target membrane (5–7). Once these minimal requirements have been satisfied, the membranes of influenza and host membrane mix to form a structure that is referred to as a hemifusion stalk and subsequently a hemifusion diaphragm, and then a fusion pore is formed and widened to allow for genome transfer (8). Although IAV and HA-mediated fusion have been widely studied, there are still questions remaining about the detailed mechanism of pore formation, specifically the timescale and dynamics of genome transfer and how the composition of the target membrane affects efficient transfer.

The kinetics of content mixing have been studied in many in vitro reductionist systems that utilize model membranes as a proxy for cells. These simplified membranes enable researchers to control target membrane compositions to

Submitted April 25, 2021, and accepted for publication September 9, 2021.
*Correspondence: sboxer@stanford.edu
Editor: Ilya Levental.
https://doi.org/10.1016/j.bpj.2021.09.023

systematically study the impact of various membrane components on viral fusion. Cholesterol is one membrane component that is of significant interest as it comprises roughly 30–40 mol% of the plasma and endosomal membranes (9); it is hypothesized that the cholesterol-rich regions of host membranes facilitate viral fusion peptide engagement, which can promote membrane fusion (10–12), and vesicle fusion studies have found that cholesterol enhances fusion and pore formation (13–15). In bulk studies, in which fusion between virions and vesicles is observed by fluorescence dequenching and an overall increase in fluorescence signal, cholesterol speeds the rates of IAV lipid mixing (hemifusion) and content mixing (pore formation) (16). However, ensemble measurements report average behavior for a large number of particles, and the readout for content mixing can be confounded by issues like vesicle rupture, content leakage, and viral or target vesicle aggregation.

To address the shortcomings of bulk measurements, efforts have been made toward developing single-virus assays to monitor the kinetics of lipid and content mixing (6,17–19). These single-virus assays can characterize the heterogeneity in viral fusion events and short-lived kinetic intermediates that are typically lost in bulk averaging studies. In fluorescence-based experimental architectures, virions are lipid- and/or content-labeled with self-quenched concentrations of fluorescent dyes. Content-labeling virions with sufficient amounts of dye to be useful involves a long incubation period (anywhere from 16 h to 2 days) in a water-soluble dye (6,20,21). The labeling process is specific to each virus, and it requires significant optimization to successfully incorporate dyes while ensuring that labels do not impact viral infectivity. In most prior work, labeled virions were fused to a supported lipid bilayer (SLB) formed on a solid support, where content mixing is detected as dequenching, followed by a sharp drop in fluorescence intensity as the content dye diffuses away.

Although SLBs may be a suitable target for studies of outer leaflet mixing, it is not clear how the solid support affects engagement of the inner leaflet. Some single-virus membrane fusion studies attempt to mitigate this concern by mounting SLBs on dextran cushions to provide a hydrated layer between the membrane and the glass surface (6,20). Even though cushion-mounted SLBs have been shown to be fluid through fluorescence recovery after photobleaching, polymer-cushioned membranes are susceptible to structural defects and incomplete cushion formation (22). Similar issues arise in models for SNARE-mediated membrane fusion where tethered bilayers, held some distance from the solid support, have been used to surmount this limitation (23). Additionally, as dye-labeled viruses fuse to a target SLB and the membranes mix, the composition of the target membrane changes over time, as evidenced by the build-up of fluorescence background in the SLB. This change in SLB composition may affect the target membrane composition for neighboring events, which would make it difficult to objectively study how target membrane composition affects viral fusion kinetics.

To address these concerns about SLB architectures, we and others have developed single-virus lipid mixing assays in which viruses fuse to tethered vesicles instead of SLBs (24–26). In these assays, vesicles are tethered to labeled virions through either sialic acid receptors or synthetic DNA-lipid tethers, and single lipid mixing events are detected by fluorescence microscopy. Because individual virions are tethered to different vesicles, the target membrane composition does not change before a lipid mixing event occurs, and dye labels stay confined to each virus-vesicle pair after mixing. For IAV, it has been shown using target vesicles from 30 to 100 nm in diameter that the overall starting curvature of the target membrane does not affect the rate of single-virus lipid mixing (27). As long as surface passivation is optimized to prevent nonspecific binding, vesicles offer an attractive alternative to SLBs as host membrane mimics.

To avoid the process of adding a self-quenched concentration of fluorescently tagged lipids to the viral envelope, we previously created a new version of the single-virus lipid mixing assay in which the experimental readout for viral fusion is fluorescence dequenching of lipid-labeled target vesicles. Using this assay, we found that the target membrane cholesterol enhances the efficiency of IAV lipid mixing but has no effect on the rate (28). Here, we present a single-virus content-mixing assay that utilizes content-labeled vesicles to eliminate the difficult process of content-labeling virions. Employing vesicles as target membranes enables the characterization of content leakage dynamics that cannot be observed in typical SLB architectures.

MATERIALS AND METHODS

Materials

Palmitoyl oleoyl phosphatidylcholine (POPC), dioleoyl phosphatidylethanolamine (DOPE), and cholesterol were purchased from Avanti Polar Lipids (Alabaster, AL). Texas Red-1,2-dihexadecanoyl-*sn*-glycero-3-phosphoethanolamine (TR-DHPE), Oregon Green-1,2-dihexadecanoyl-*sn*-glycero-3-phosphoethanolamine (OG-DHPE), fatty acid-depleted bovine serum albumin (BSA), and NeutrAvidin were purchased from Thermo Fisher Scientific (Waltham, MA). Sulforhodamine B (SRB), Sepharose CL-4B, and disialoganglioside GD1a from bovine brain (Cer-Glc-Gal(NeuAc)-GalNAc-Gal-NeuAc) were purchased from Sigma-Aldrich (St. Louis, MO). Chloroform, methanol, HEPES buffer, and buffer salts were obtained from Fisher Scientific (Pittsburgh, PA) and Sigma-Aldrich. Polydimethylsiloxane was obtained from Ellsworth Adhesives (Hayward, CA). Poly(L-lysine)-graft-poly(ethylene glycol) and Poly(L-lysine)-graft-poly(ethylene glycol) biotin were purchased from SuSoS (Dübendorf, Switzerland).

Buffers

The following buffers were used: vesicle buffer: 10 mM NaH_2PO_4, 90 mM sodium citrate, and 150 mM NaCl (pH 7.4); fusion buffer: 10 mM NaH_2PO_4, 90 mM sodium citrate, and 150 mM NaCl (pH 5.1); HB

buffer: 20 mM HEPES and 150 mM NaCl (pH 7.2); and content buffer: 30 mM SRB, 10 mM NaH_2PO_4, 90 mM sodium citrate, and 120 mM NaCl (pH 7.4).

Microscopy

Epifluorescence micrographs were acquired with a Nikon Ti-U microscope using a 100× oil immersion objective (NA = 1.49) (Nikon Instruments, Melville, NY), a Spectra-X LED Light Engine (Lumencor, Beaverton, OR) for illumination, and an Andor iXon 897 EMCCD camera (Andor Technologies, Belfast, UK) with 16-bit image settings. Images were captured with Metamorph software (Molecular Devices, Sunnyvale, CA). See Supporting materials and methods for additional microscopy information.

DNA-lipid and biotin-DNA preparation

DNA-lipids (see Table S1 for sequences) used to surface tether viruses were synthesized as previously described (29). Biotinylated DNA was synthesized by the Protein and Nucleic Acid Facility at Stanford University (Stanford, CA) and diluted to the desired concentration in deionized water. All DNA oligos were stored at −20°C.

Influenza virus preparation

IAV (strain X-31, A/Aichi/68, H3N2) was purchased from Charles River Laboratories (Wilmington, MA). Virus was pelleted in HB buffer by centrifugation at 21,130 rcf for 50 min and resuspended in fresh HB buffer. DNA-lipids were incorporated into the IAV envelope by incubating virus sample at 4°C on ice overnight as previously described (24,28). IAV is a Biosafety Level 2 agent and was handled following an approved biosafety protocol at Stanford University.

Vesicle preparation

Lipid mixtures were prepared in chloroform and dried down to a film under argon gas, and the film was dried under house vacuum for at least 3 h. Mixtures contained 10–40 mol% cholesterol, 20 mol% DOPE, 2 mol% GD1a, and remaining mol% POPC (see Table S1). Dried lipid films were resuspended in content buffer by vortexing, and large unilamellar vesicles with a nominal diameter of 100 nm were prepared by extrusion. Vesicle suspensions were stored at 4°C and used within a week. To incorporate DNA-lipids into the outer leaflet of vesicles composed of 10% cholesterol, DNA-lipids were added to a vesicle suspension and incubated overnight at 4°C, as described in previous studies (24,30). Immediately before use in a content-mixing experiment, vesicles were purified from free SRB dye on a CL-4B size exclusion column and equilibrated with vesicle buffer. After equilibration, vesicles were used within 4 hrs.

Surface and architecture preparation

The single-virus content-mixing architecture was prepared as described in Fig. 1. In a microfluidic flow cell (see Supporting materials and methods for details), glass slides were functionalized as previously described (28). Next, 5 μL of IAV in HB buffer (roughly 5.4 nM) displaying DNA sequence A′ (antisense to A) were introduced to the flow cell and tethered to the substrate. For experiments to vesicles with 10% cholesterol and antibody content-mixing experiments, IAV also displayed DNA sequence B (Fig. S1). After rinsing the flow cell with vesicle buffer, the surface was further passivated by incubating 10 μL of BSA (1 g/L) for at least 10 min to prevent nonspecific binding of the added target vesicles. Finally, 2–3 μL of ∼100 nm diameter vesicles displaying GD1a and containing content buffer were introduced (2.8 μM nominal total lipid concentration). Vesicles with 10% cholesterol displayed both GD1a and DNA sequence B′ (antisense to B). Content vesicles were allowed to bind for 5–10 min to control surface density and ensure spatial separation between particles. Excess unbound vesicles and BSA were removed by rinsing with vesicle buffer.

Content mixing assay

Fluorescence microscopy was used to collect a video micrograph image stream of 1200 frames at a rate of 3.47 frames/s. After the image stream was started, the pH of flow cell was rapidly exchanged from 7.4 to 5.1 using fusion buffer. In a separate experiment, tethered vesicles that contained a pH indicator (2 mol% OG-DHPE) were used to calibrate the exchange time of fusion buffer (2–3 s). The times between the lowering of pH to dequenching and/or content escape were extracted using custom MATLAB (The MathWorks, Natick, MA) scripts, as described previously (24,28). The wait times from fluorescence traces with more than one dequenching event are excluded from cumulative distribution functions (CDFs).

Single-virus binding assay

IAV was labeled with TR-DHPE using methods previously described (24,31). Labeled IAV was incubated with various solutions of monoclonal antibodies for 2 h at 22°C. SLBs (67.9% POPC, 20% DOPE, 10% cholesterol, 2% GD1a, and 0.1% OG-DHPE) were formed through vesicle fusion. Antibody-bound virions were introduced to this bilayer and allowed to bind for 60 s. Unbound virions were rinsed away using vesicle buffer, and the resulting number of virions was quantified through spot analysis of fluorescence micrographs using MATLAB scripts. See Supporting materials and methods for more details.

RESULTS

Single-virus content-mixing assay

We created an assay to observe single-virus content-mixing events that does not require the difficult and perturbative process of labeling viral contents (Fig. 1). First, IAV particles with no fluorescent label are incubated with an aqueous suspension of DNA-lipids. After at most a few DNA-lipids have incorporated into the IAV envelope (28), virions are tethered to a passivated glass slide in a polydimethylsiloxane microfluidic flow cell through DNA hybridization. It is essential that the surface be completely passivated to prevent nonspecific adhesion of virus particles or vesicles. Next, target vesicles containing a self-quenched concentration of the water-soluble content dye SRB and displaying GD1a glycolipid receptors are introduced at a dilute concentration and allowed to bind to the tethered IAVs. Vesicles are nominally 100 nm in diameter to ensure that mixing with influenza A virions would roughly double the volume of the dye and result in dequenching. We have previously shown using dynamic light scattering that varying the amount of cholesterol in the target membrane does not significantly change the size of vesicles (28). We note that recent evidence has shown that extrusion yields a fraction of vesicles that are multilamellar (32), although not under our preparation conditions and for these specific compositions.

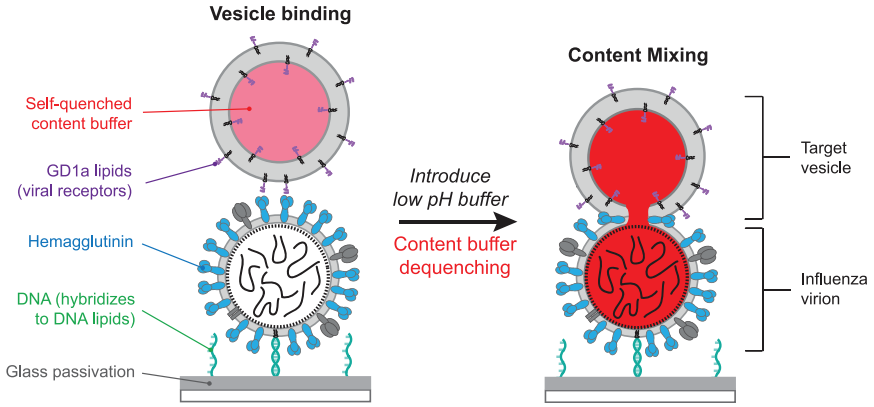

FIGURE 1 Schematic of single-virus content-mixing assay. Influenza A virions are tethered to a passivated (*gray*), DNA-functionalized glass coverslip in a microfluidic device through DNA hybridization (*green*). Target vesicles containing a self-quenched concentration of SRB content buffer (*red*) and GD1a glycolipids (*purple*) bind to HA (*blue*) of influenza A virions. For vesicles composed of 10 mol% cholesterol, vesicles also displayed a small number of DNA-lipids that were orthogonal to the surface-tethering sequences (Fig. S1). Once vesicles are bound, low pH buffer is exchanged to trigger fusion, and fluorescence dequenching occurs as the contents between target vesicle and virus mix. To see this figure in color, go online.

We observed that vesicles composed of 20–40 mol% cholesterol and 2 mol% GD1a bind stably to tethered IAV. However, the interaction of vesicles composed of 10 mol% cholesterol with IAV is reversible and transient, which causes vesicles to become unbound during the process of rapid buffer exchange, so they cannot be reliably monitored. The reversible binding of 10 mol% cholesterol vesicles, but stable binding of 20–40 mol% cholesterol vesicles, is consistent with previous work, which showed that higher cholesterol levels increase IAV binding avidity, likely because of cholesterol/GD1a cluster formation (33). Therefore, to stably tether 10 mol% cholesterol target vesicles, we added an orthogonal DNA-lipid to target vesicles to hybridize with a complementary sequence in the IAV envelope (sense/antisense sequence B, see Table S1 and Fig. S1). As previously shown, DNA-lipid incorporation into vesicles and the IAV envelope does not follow Poisson statistics (24,28,30). Of vesicles that display at least one DNA-lipid, the median number incorporated is four DNA-lipids per vesicle (Fig. S1).

Once content-labeled vesicles are bound to IAV at a high, yet still spatially resolvable density (detected by their weak residual SRB fluorescence), unbound vesicles are rinsed from the flow cell using a low flow rate to prevent bursting or leakage of content-labeled vesicles. Next, the pH of the flow cell is exchanged from pH 7.4 to 5.1, occurring over 2–3 s (calibrated in virus-free samples using OG-DHPE-labeled vesicles as a pH sensor). This rapid buffer exchange is also conducted at a flow rate that does not lead to leakage or bursting of content-labeled vesicles. The fluorescence intensity, or SRB signal, of each content-labeled vesicle is monitored over time through a video micrograph collected for 1200 frames at 288 ms/frame.

Upon lowering the pH, we observed several types of fluorescence time traces and classified them into four categories: content mixing (Fig. 2 *A*), content mixing followed by content loss (Fig. 2 *B*), content loss (no evidence of mixing, Fig. 2 *C*), and no change. For the majority of traces (70–80%), no change was detected. We describe the first three categories in more detail below.

In a content-mixing trace, after the pH is lowered to 5.1, the vesicle displays dequenching because of dilution of contents with the interior of the influenza virion. This interpretation of content mixing is consistent with previous studies of vesicle fusion between two vesicles (34). After the content-mixing event, the fluorescence intensity of the vesicle stays constant (Fig. 2 *A*). Roughly 3–15% of traces were classified as content mixing, which is described in more detail below.

We describe the second category as content mixing followed by content loss, which made up 1.0–1.5% of traces. After the pH is lowered to 5.1, these vesicles display dequenching because of content mixing. After the dequenching event, there is a sustained period of constant fluorescence, followed by content loss, as indicated by a sharp decrease in fluorescence intensity (Fig. 2 *B*). For all vesicles that undergo content mixing and content mixing followed by content loss, the wait time is defined as τ_{CM}, or the time from the pH drop to the content-mixing event. The interval after mixing in which the fluorescence intensity stays constant is defined as $\tau_{CM\rightarrow CL}$, or the time from the content-mixing event to content loss.

We refer to the final category of time traces as content loss only (no mixing). In these vesicles, after the pH is lowered to 5.1, no increase in fluorescence characteristic of content-mixing dequenching is detected, and there is a sharp decrease in fluorescence intensity, which corresponds to content loss (Fig. 2 *C*). The time to content loss is defined as τ_{CL}, or the time from pH drop to content loss. For most content-loss traces, content dequenching as a result of dilution with the external buffer solution occurs on a timescale that is faster than the video micrograph collection frame rate (288 ms/frame).

Content mixing, with and without subsequent content loss, is only observed at low pH in the presence of IAV. At neutral pH, we do not observe any instances of content mixing followed by content loss (Fig. S2). When content-labeled vesicles are tethered to glass through DNA hybridization in the absence of IAV, we do not observe any content mixing, or content mixing followed by content loss (Fig. S2).

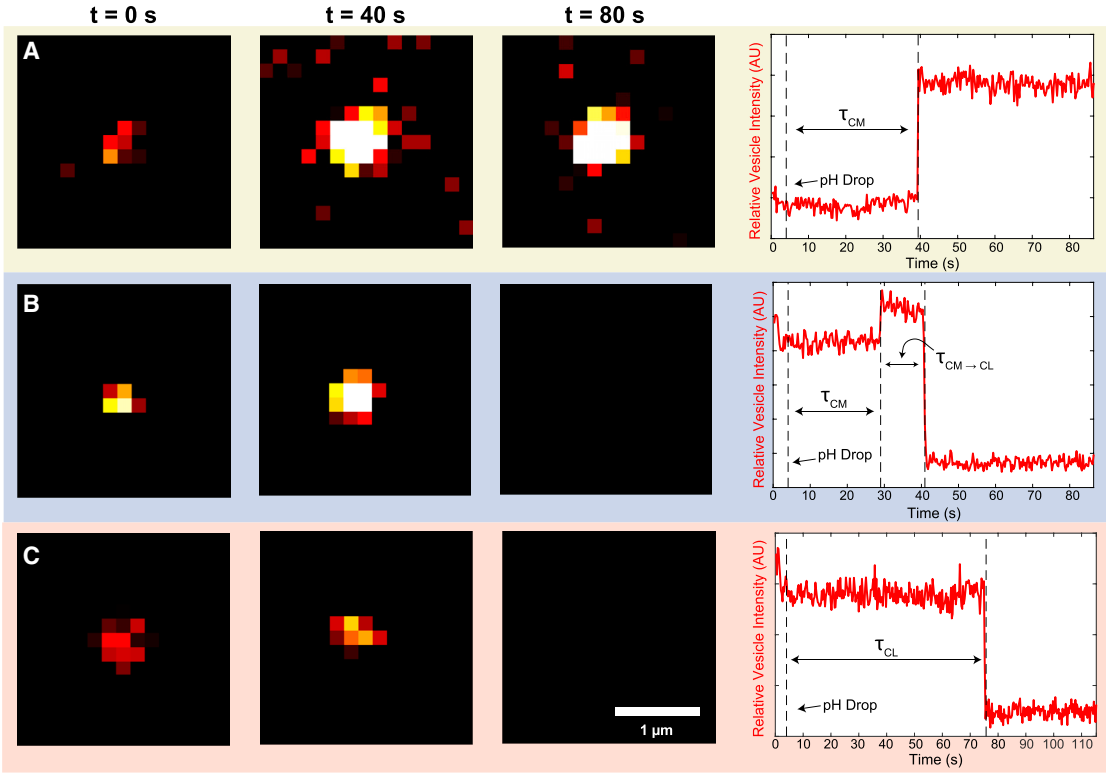

FIGURE 2 Lowering the pH triggers virion-vesicle content mixing detected by fluorescence dequenching and content loss indicated by dye disappearance. When the pH is lowered, some vesicles exhibit a change in fluorescence intensity; these traces were classified into three categories. Shown are example microscope images of individual content-labeled vesicles bound to surface-tethered influenza virions (*left*). At pH 7.4, content-labeled vesicles are dim but detectable. Representative observed fluorescence intensity time traces correspond to single content-labeled vesicles (*right*). (*A*) Content mixing: after the pH is lowered to 5.1, the vesicle displays dequenching due to dilution of contents with the interior of the influenza virion. After content mixing, the fluorescence intensity of the vesicle-virion complex stays constant. (*B*) Content mixing followed by content loss: after the pH is lowered to 5.1, the vesicle displays dequenching due to content mixing. After the dequenching event, there is a sustained period of constant fluorescence, followed by content loss, as indicated by a sharp decrease in fluorescence intensity. For both (*A* and *B*), the wait time is defined as τ_{CM}, or the time from the pH drop to the content-mixing event. The time from content mixing to loss, or $\tau_{CM} \rightarrow \tau_{CL}$, is defined as the time from the content-mixing event to content loss. (*C*) Content loss, no detectable mixing: after the pH is lowered to 5.1, no content mixing event is detected, and the content-labeled vesicle undergoes content loss. For (*C*), content dequenching occurs more quickly than the collection frame rate (288 ms/frame). The time to content loss, or τ_{CL}, is defined as the time from pH drop to content loss. To see this figure in color, go online.

Cholesterol enhances the efficiency of content mixing but not the rate

To understand how target membrane cholesterol affects the rate of content mixing, we took τ_{CM} values for each target vesicle composition and plotted them in individual CDFs (Fig. S3). CDFs contain τ_{CM} values from vesicles that underwent content mixing, as well as content-mixing events that were followed by content loss. When we compared the CDFs for each composition, the rates of content mixing do not change significantly as target membrane cholesterol increases (Fig. 3 *A*).

The number of vesicles that undergo content mixing, or N_{CM}, can be divided by the total vesicles in a field of view, or N, to yield the content-mixing efficiency. Target membrane cholesterol enhances the efficiency of content mixing (Fig. 3 *B*). For all target membrane compositions tested, content mixing was a slower and less efficient process than lipid mixing, which suggests that a large fraction of lipid mixing events that occur do not proceed to full fusion (see Figs. S4 and S5 for direct comparisons of content mixing and previously published lipid mixing kinetics).

Cholesterol increases the number of content-mixing events that result in stable pore formation

We quantified the rate and frequency of content-mixing events that were followed by content loss. The frequency was calculated by dividing the number of content-mixing traces that result in content loss, or $N_{CM \rightarrow CL}$, by the total number of vesicles that undergo content mixing, or N_{CM}. We compared this fraction, $N_{CM \rightarrow CL}/N_{CM}$, for vesicles composed of 10–40 mol% cholesterol and found that target membrane cholesterol decreases the fraction of content-mixing events that result in eventual content loss (Fig. 4 *A*). The $\tau_{CM \rightarrow CL}$ intervals for each composition were plotted in

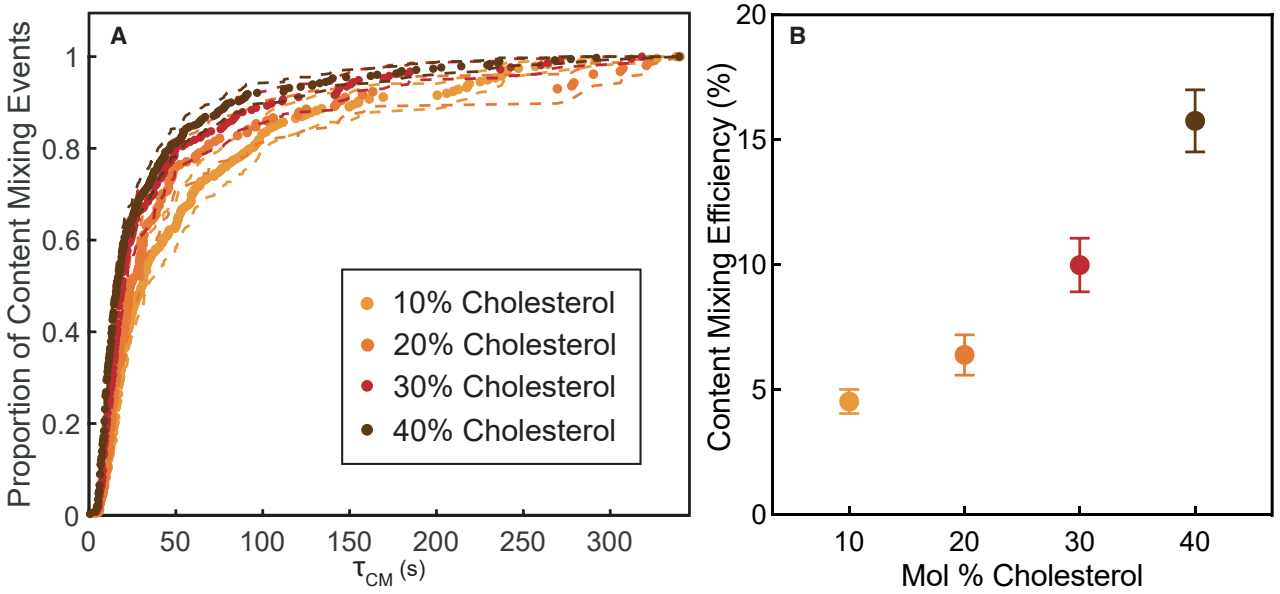

FIGURE 3 Cholesterol enhances the efficiency of single-particle IAV content mixing but does not affect the rate. (*A*) Wait times from pH drop to content mixing (τ_{CM}) for individual content-mixing events are plotted as CDFs. From 10 to 40 mol% cholesterol, the rate of IAV content mixing is the same within bootstrap resampling error (95% confidence intervals, *dashed lines*). (*B*) The relative efficiency, or fraction of target vesicles that undergo content mixing, increases 3.5-fold as the mole percentage of cholesterol in target vesicles increases. Points represent the efficiency value ± bootstrap resampling error. The number of content-mixing events for 10, 20, 30, and 40 mol% cholesterol is 238/5250, 157/2458, 215/2153, and 380/2411, respectively. The total number of vesicles analyzed is proportional to the number of individual experiments executed and not because of inherent differences in binding behavior. Kinetic data for each composition were compiled from at least four different independent viral preparations. To see this figure in color, go online.

individual CDFs and compared, but $N_{CM\rightarrow CL}$ values for high cholesterol-containing vesicles were too low to observe any significant difference between compositions (Fig. S6).

Kinetics of content loss are independent of membrane composition

Next, we analyzed the rate and frequency of vesicles that displayed content loss (with no content-mixing event detected) for each target membrane cholesterol composition. Content loss is a competing process to content mixing; in our assay, once vesicles undergo content loss, we are unable to monitor whether a productive mixing event occurs later. As a result, we sought to understand whether the frequency of content-loss events was cholesterol dependent, which could be a confounding factor in content-mixing and loss efficiencies.

The frequency of content-loss events was calculated by dividing the number of vesicles that were classified as content loss, N_{CL}, by the total number of vesicles monitored, N. When we compared the frequency of content loss, N_{CL}/N, for vesicles composed of 10–40 mol% cholesterol, we found that altering target membrane cholesterol does not have a significant effect (Fig. 4 *B*).

The τ_{CL} intervals for each composition were plotted in individual CDFs (Fig. S7) and compared, and cholesterol also did not have a significant effect on the rate of content loss. These findings indicate that the process that leads to content loss is not affected by membrane cholesterol composition. Although we do detect a few content-loss events when the vesicles are exchanged with neutral pH buffer, there are significantly more content-loss events at low pH when content-labeled vesicles are tethered to IAV (Fig. S8). Because of this background of content-loss events that take place when flow cells are changed with neutral pH buffer, all experiments were rinsed with a standardized amount of buffer.

Because content loss was independent of target membrane composition, we hypothesized that the events could be derived from IAV HA engagement with target membranes. To test the role of HA engagement in content loss, we neutralized HAs by introducing monoclonal antibodies to bind to the HA receptor binding domain. Antibodies were not fluorescently labeled; the extent of antibody coverage was determined through a functional single-virus binding assay based on previous studies (26,33) in which virions were labeled with TR-DHPE and incubated with various concentrations of antibody solutions. Virions were then introduced to a microfluidic flow cell containing an SLB that was composed of 2 mol% GD1a, and the number of virions bound per microscope FOV was quantified through spot analysis of fluorescence micrographs. We determined that incubating IAV with two concentrations of monoclonal antibodies, 0.05 and 0.5 mg/mL, led to a roughly 50 and 100% reduction of IAV binding in comparison to IAV with no antibodies (Fig. S9).

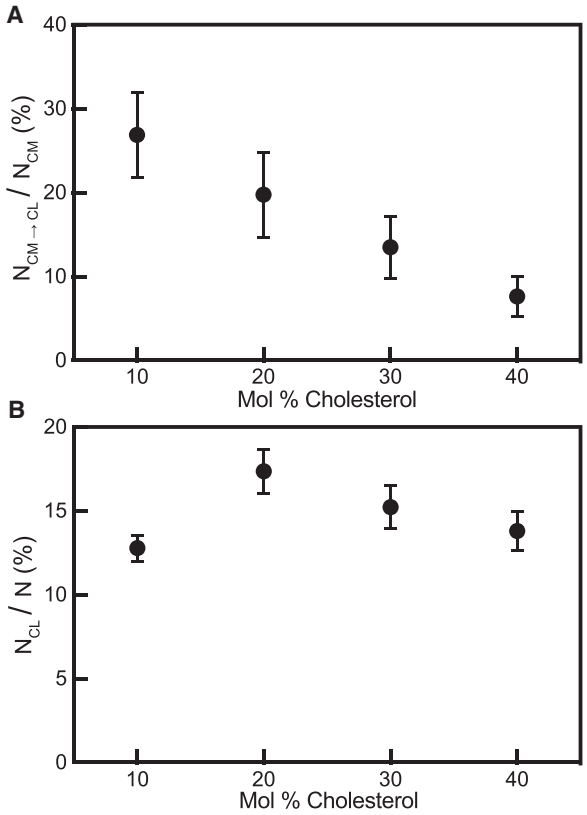

FIGURE 4 Cholesterol decreases the number of content-mixing events that result in content loss but has no effect on the frequency of content loss. (*A*) Target membrane cholesterol decreases the fraction of content-mixing events that result in content loss. The fraction of content-mixing events that result in content loss for 10, 20, 30, and 40 mol% cholesterol is 64/238, 31/157, 29/215, and 29/380, respectively. (*B*) Increasing target membrane cholesterol has no significant effect on the fraction of vesicles that undergo content loss with no previous mixing event. The number of content-loss events for 10, 20, 30, and 40 mol% cholesterol is 724/5250, 427/2458, 328/2153, and 333/2411, respectively. Points represent the fraction ± bootstrap resampling error.

Next, we utilized the single-virus content-mixing assay to understand how neutralizing HAs through antibody binding affects content mixing and content loss. Because antibodies prevent IAV from binding to GD1a, target vesicles were bound to IAV through DNA-lipid hybridization (median of four DNA-lipids/vesicle, Fig. S1). Antibodies decreased the content-mixing efficiency of IAV to target vesicles composed of 10 and 40 mol% cholesterol (Fig. S10), which is consistent with previous studies that showed that neutralizing antibodies decrease the efficiency of IAV lipid mixing (35). Additionally, neutralizing HA with antibodies decreased the frequency of content-loss events for both target vesicle compositions (Fig. 5). A similar antibody-dependent reduction in the number of content-loss events was also observed for vesicles that were only tethered to IAV with DNA-lipids (no GD1a present in membranes), which suggests that the HA-GD1a interaction at low pH does not play a role in membrane breakage (Fig. S11).

DISCUSSION

We designed a single-virus content-mixing assay that employs content-labeled vesicles as target membranes and does not require the process of labeling viral contents. By systematically altering the composition of vesicles used in this assay, we found that cholesterol enhances the efficiency of IAV content mixing but has no effect on the rate. The effect of target membrane cholesterol on content mixing is unsurprising given our previous finding that cholesterol also increases the efficiency of lipid mixing and has no effect on the rate (28). If there is just one rate-determining step between IAV lipid mixing and content mixing as is widely believed (6), it follows that the rate of content mixing would be similarly unaffected by target membrane cholesterol. The enhancement in content-mixing efficiency because of cholesterol is consistent with other IAV fusion studies that varied target membrane composition (16) and also further supports the hypothesis that the negative spontaneous curvature (SC) of cholesterol stabilizes the formation of the highly curved structure that is necessary for pore formation and widening (36,37).

Cryo-electron tomograms of IAV fusing to vesicles have suggested that the negative SC of target membrane cholesterol acts as a "pathway switch," in which membranes with less than 31 mol% cholesterol go through a "rupture-insertion" pathway as opposed to the canonical, nonleaky hemifusion stalk pathway (38). A subsequent study utilized a poration assay to expand on this theory by monitoring the influx of dye into giant unilamellar vesicles (GUVs) during IAV fusion. The assay concluded that the trend in membrane rupture was generalizable to target membrane SC; when SC was below -0.20 nm^{-1}, fusion was predominantly nonleaky, whereas above that threshold, most fusion events were leaky (39). Our observations are generally in agreement with the hypothesis that the negative SC of cholesterol decreases the number of content-mixing events that lead to content loss. However, our results suggest that increasing cholesterol stabilizes fusion pore formation in a more gradual manner, rather than a dramatic shift when SC is below -0.20 nm^{-1} (or above 20 mol% cholesterol; see (28) for SC calculations of compositions used in this study). We hypothesize that our results diverge from previous studies because of differences in assay architecture. In the content-mixing assay we present here, we monitor the real-time kinetics of content mixing and content loss of single fusion events, whereas in the GUV poration assay, multiple virions could fuse to one vesicle, and fusion events were not counted until 10 min after low pH was introduced.

Conductance measurements have suggested that membrane permeability temporarily increases in a composition-dependent manner during the process of fusion pore formation, which could lead to content loss as HA rearranges within fusing membranes (40). Additionally, computational simulations of vesicle fusion propose that

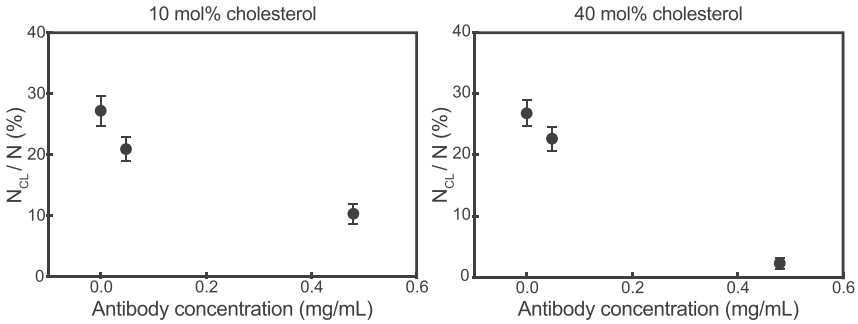

FIGURE 5 IAV antibodies decrease the frequency of content-loss events to membranes containing 10 and 40 mol% cholesterol. Influenza A virions were incubated with various concentrations of monoclonal antibodies. Content-labeled vesicles with 10 and 40 mol% cholesterol were tethered to virions through DNA-lipid hybridization, and the pH was lowered to trigger content mixing and content loss. For both target membrane compositions, the addition of antibodies to IAV decreased the frequency of content-loss events. Each data point represents the frequency of content loss ± bootstrap resampling error for at least 900 vesicles.

cholesterol decreases the water penetrability of the membrane to inhibit leaky pore formation (41).

From a viral fitness perspective, unsuccessful pore formation is undesirable because it can inhibit viral replication. However, it has been shown that influenza genome transfer for single virions is often incomplete (42), and one contributing reason may be that fusion pores are more unstable when they are formed in host membrane regions that are relatively low in cholesterol. Other enveloped viruses have been shown to preferentially fuse to the boundary of cholesterol-rich regions of host membranes (43,44), which suggests that protein-mediated pore formation for IAV may also selectively occur within or at the edges of cholesterol-enriched regions of the membrane. In this study, the target vesicle compositions do not lead to microscale domain formation and are visually homogenous through fluorescence microscopy, although the mixtures that we use have not been studied for any nanoscale phase separation. We are unaware of any method that can directly access the exact membrane composition at the areas in which fusion pores are formed and determine how this correlates with function.

Finally, it is clear from our observations that the low-pH form of HA plays a key role in IAV-facilitated content loss from content-labeled vesicles, and this action is inhibited by monoclonal antibody binding. However, because there is no way to directly characterize the structure of each individual virion-vesicle pair whose kinetics are observed, it is difficult to make any conclusions about the structural basis for content loss. In other ensemble and structural studies, HA fusion peptide engagement has been hypothesized to lead to the deformation of host membranes (39,45–49), and it is known that hydrophobic peptide insertion can lead to membrane disruption. This process could potentially create membrane gaps large enough for the content dye to escape from the vesicles in our assay.

CONCLUSIONS

Here, we present a new strategy for observing single-virus content mixing that does not require the difficult, variable, and potentially damaging process of content-labeling virions. By tethering content-labeled vesicles to IAV, we are able to characterize the effect of target membrane cholesterol on the kinetics of viral content mixing and content loss. We show that like IAV lipid mixing, the rate of IAV content mixing is not significantly changed by target membrane cholesterol, but cholesterol increases the efficiency of fusion pore formation. We also demonstrate that the engagement of the HA fusion peptide with target membranes can lead to content loss in a manner that is independent of membrane composition.

The content-mixing assay we present here could be used for studying the dynamics of pore formation for other enveloped viruses in which the viral receptor is known and can be reconstituted in a target vesicle, without requiring the process of labeling viral contents. One limitation of our study is that the content dye SRB is a much smaller molecule than the IAV genome. Directly detecting viral genome transfer in model systems is challenging, but efforts to do this are ongoing.

SUPPORTING MATERIAL

Supporting material can be found online at https://doi.org/10.1016/j.bpj.2021.09.023.

AUTHOR CONTRIBUTIONS

K.N.L. designed experiments, performed experiments, analyzed data, and co-wrote the article. S.G.B. designed experiments and co-wrote the article.

ACKNOWLEDGMENTS

The authors thank Dr. Elizabeth Webster, Prof. Robert Rawle, and Prof. Peter Kasson for helpful discussions. Monoclonal antibodies were a kind gift from Dr. Robert Webster (St. Jude's Children's Research Hospital).

K.N.L. was supported by a National Science Foundation Graduate Research Fellowship. This work was supported by National Institutes of Health grant R35 GM118044 to S.G.B.

REFERENCES

1. Chernomordik, L. V., V. A. Frolov, …, J. Zimmerberg. 1998. The pathway of membrane fusion catalyzed by influenza hemagglutinin: restriction of lipids, hemifusion, and lipidic fusion pore formation. *J. Cell Biol.* 140:1369–1382.

2. Harrison, S. C. 2015. Viral membrane fusion. *Virology.* 479–480:498–507.
3. Skehel, J. J., P. M. Bayley, …, D. C. Wiley. 1982. Changes in the conformation of influenza virus hemagglutinin at the pH optimum of virus-mediated membrane fusion. *Proc. Natl. Acad. Sci. USA.* 79:968–972.
4. Carr, C. M., and P. S. Kim. 1993. A spring-loaded mechanism for the conformational change of influenza hemagglutinin. *Cell.* 73:823–832.
5. Ivanovic, T., and S. C. Harrison. 2015. Distinct functional determinants of influenza hemagglutinin-mediated membrane fusion. *eLife.* 4:e11009.
6. Floyd, D. L., J. R. Ragains, …, A. M. van Oijen. 2008. Single-particle kinetics of influenza virus membrane fusion. *Proc. Natl. Acad. Sci. USA.* 105:15382–15387.
7. Danieli, T., S. L. Pelletier, …, J. M. White. 1996. Membrane fusion mediated by the influenza virus hemagglutinin requires the concerted action of at least three hemagglutinin trimers. *J. Cell Biol.* 133:559–569.
8. Chernomordik, L. V., J. Zimmerberg, and M. M. Kozlov. 2006. Membranes of the world unite! *J. Cell Biol.* 175:201–207.
9. van Meer, G., D. R. Voelker, and G. W. Feigenson. 2008. Membrane lipids: where they are and how they behave. *Nat. Rev. Mol. Cell Biol.* 9:112–124.
10. Lai, A. L., A. E. Moorthy, …, L. K. Tamm. 2012. Fusion activity of HIV gp41 fusion domain is related to its secondary structure and depth of membrane insertion in a cholesterol-dependent fashion. *J. Mol. Biol.* 418:3–15.
11. Meher, G., S. Sinha, …, H. Chakraborty. 2019. Cholesterol modulates membrane properties and the interaction of gp41 fusion peptide to promote membrane fusion. *J. Phys. Chem. B.* 123:7113–7122.
12. Meher, G., S. Bhattacharjya, and H. Chakraborty. 2019. Membrane cholesterol modulates oligomeric status and peptide-membrane interaction of severe acute respiratory syndrome coronavirus fusion peptide. *J. Phys. Chem. B.* 123:10654–10662.
13. Lee, D. E., M. G. Lew, and D. J. Woodbury. 2013. Vesicle fusion to planar membranes is enhanced by cholesterol and low temperature. *Chem. Phys. Lipids.* 166:45–54.
14. Kreutzberger, A. J. B., V. Kiessling, and L. K. Tamm. 2015. High cholesterol obviates a prolonged hemifusion intermediate in fast SNARE-mediated membrane fusion. *Biophys. J.* 109:319–329.
15. Stratton, B. S., J. M. Warner, …, B. O'Shaughnessy. 2016. Cholesterol increases the openness of SNARE-mediated flickering fusion pores. *Biophys. J.* 110:1538–1550.
16. Domanska, M. K., D. Wrona, and P. M. Kasson. 2013. Multiphasic effects of cholesterol on influenza fusion kinetics reflect multiple mechanistic roles. *Biophys. J.* 105:1383–1387.
17. Wessels, L., M. W. Elting, …, K. Weninger. 2007. Rapid membrane fusion of individual virus particles with supported lipid bilayers. *Biophys. J.* 93:526–538.
18. Otterstrom, J., and A. M. van Oijen. 2013. Visualization of membrane fusion, one particle at a time. *Biochemistry.* 52:1654–1668.
19. Nathan, L., and S. Daniel. 2019. Single virion tracking microscopy for the study of virus entry processes in live cells and biomimetic platforms. *Adv. Exp. Med. Biol.* 1215:13–43.
20. Ivanovic, T., R. Rozendaal, …, S. C. Harrison. 2012. Kinetics of proton transport into influenza virions by the viral M2 channel. *PLoS One.* 7:e31566.
21. Costello, D. A., J. K. Millet, …, S. Daniel. 2013. Single particle assay of coronavirus membrane fusion with proteinaceous receptor-embedded supported bilayers. *Biomaterials.* 34:7895–7904.
22. Watkins, E. B., R. J. El-khouri, …, T. L. Kuhl. 2011. Structure and thermodynamics of lipid bilayers on polyethylene glycol cushions: fact and fiction of PEG cushioned membranes. *Langmuir.* 27:13618–13628.
23. Rawle, R. J., B. van Lengerich, …, S. G. Boxer. 2011. Vesicle fusion observed by content transfer across a tethered lipid bilayer. *Biophys. J.* 101:L37–L39.
24. Rawle, R. J., S. G. Boxer, and P. M. Kasson. 2016. Disentangling viral membrane fusion from receptor binding using synthetic DNA-lipid conjugates. *Biophys. J.* 111:123–131.
25. Rawle, R. J., E. R. Webster, …, S. G. Boxer. 2018. pH dependence of Zika membrane fusion kinetics reveals an off-pathway state. *ACS Cent. Sci.* 4:1503–1510.
26. Delaveris, C. S., E. R. Webster, …, C. R. Bertozzi. 2020. Membrane-tethered mucin-like polypeptides sterically inhibit binding and slow fusion kinetics of influenza A virus. *Proc. Natl. Acad. Sci. USA.* 117:12643–12650.
27. Pabis, A., R. J. Rawle, and P. M. Kasson. 2020. Influenza hemagglutinin drives viral entry via two sequential intramembrane mechanisms. *Proc. Natl. Acad. Sci. USA.* 117:7200–7207.
28. Liu, K. N., and S. G. Boxer. 2020. Target membrane cholesterol modulates single influenza virus membrane fusion efficiency but not rate. *Biophys. J.* 118:2426–2433.
29. Chan, Y.-H. M., B. van Lengerich, and S. G. Boxer. 2008. Lipid-anchored DNA mediates vesicle fusion as observed by lipid and content mixing. *Biointerphases.* 3:FA17–FA21.
30. van Lengerich, B., R. J. Rawle, …, S. G. Boxer. 2013. Individual vesicle fusion events mediated by lipid-anchored DNA. *Biophys. J.* 105:409–419.
31. Rawle, R. J., A. M. Villamil Giraldo, …, P. M. Kasson. 2019. Detecting and controlling dye effects in single-virus fusion experiments. *Biophys. J.* 117:445–452.
32. Scott, H. L., A. Skinkle, …, F. A. Heberle. 2019. On the mechanism of bilayer separation by extrusion, or why your LUVs are not really unilamellar. *Biophys. J.* 117:1381–1386.
33. Goronzy, I. N., R. J. Rawle, …, P. M. Kasson. 2018. Cholesterol enhances influenza binding avidity by controlling nanoscale receptor clustering. *Chem. Sci. (Camb.).* 9:2340–2347.
34. Kyoung, M., A. Srivastava, …, A. T. Brunger. 2011. In vitro system capable of differentiating fast Ca2+-triggered content mixing from lipid exchange for mechanistic studies of neurotransmitter release. *Proc. Natl. Acad. Sci. USA.* 108:E304–E313.
35. Otterstrom, J. J., B. Brandenburg, …, A. M. van Oijen. 2014. Relating influenza virus membrane fusion kinetics to stoichiometry of neutralizing antibodies at the single-particle level. *Proc. Natl. Acad. Sci. USA.* 111:E5143–E5148.
36. Churchward, M. A., T. Rogasevskaia, …, J. R. Coorssen. 2008. Specific lipids supply critical negative spontaneous curvature–an essential component of native Ca2+-triggered membrane fusion. *Biophys. J.* 94:3976–3986.
37. Chernomordik, L. V., and M. M. Kozlov. 2008. Mechanics of membrane fusion. *Nat. Struct. Mol. Biol.* 15:675–683.
38. Chlanda, P., E. Mekhedov, …, J. Zimmerberg. 2016. The hemifusion structure induced by influenza virus haemagglutinin is determined by physical properties of the target membranes. *Nat. Microbiol.* 1:16050.
39. Haldar, S., E. Mekhedov, …, J. Zimmerberg. 2018. Lipid-dependence of target membrane stability during influenza viral fusion. *J. Cell Sci.* 132:jcs218321.
40. Frolov, V. A., A. Y. Dunina-Barkovskaya, …, J. Zimmerberg. 2003. Membrane permeability changes at early stages of influenza hemagglutinin-mediated fusion. *Biophys. J.* 85:1725–1733.
41. Bu, B., M. Crowe, …, D. Li. 2018. Cholesterol suppresses membrane leakage by decreasing water penetrability. *Soft Matter.* 14:5277–5282.
42. Jacobs, N. T., N. O. Onuoha, …, A. C. Lowen. 2019. Incomplete influenza A virus genomes occur frequently but are readily complemented during localized viral spread. *Nat. Commun.* 10:3526.
43. Yang, S.-T., V. Kiessling, …, L. K. Tamm. 2015. HIV gp41-mediated membrane fusion occurs at edges of cholesterol-rich lipid domains. *Nat. Chem. Biol.* 11:424–431.

44. Yang, S. T., V. Kiessling, and L. K. Tamm. 2016. Line tension at lipid phase boundaries as driving force for HIV fusion peptide-mediated fusion. *Nat. Commun.* 7:11401.

45. Jiricek, R., G. Schwarz, and T. Stegmann. 1997. Pores formed by influenza hemagglutinin. *Biochim. Biophys. Acta.* 1330:17–28.

46. Blumenthal, R., and S. J. Morris. 1999. The influenza haemagglutinin-induced fusion cascade: effects of target membrane permeability changes. *Mol. Membr. Biol.* 16:43–47.

47. Epand, R. M., and R. F. Epand. 2000. Modulation of membrane curvature by peptides. *Biopolymers.* 55:358–363.

48. Lee, K. K. 2010. Architecture of a nascent viral fusion pore. *EMBO J.* 29:1299–1311.

49. Shangguan, T., D. Alford, and J. Bentz. 1996. Influenza-virus-liposome lipid mixing is leaky and largely insensitive to the material properties of the target membrane. *Biochemistry.* 35:4956–4965.

Biophysical Journal, Volume *120*

Supplemental information

Single-virus content-mixing assay reveals cholesterol-enhanced influenza membrane fusion efficiency

Katherine N. Liu and Steven G. Boxer

Supplemental Information

Single-virus content mixing measurements show cholesterol enhances the efficiency of influenza A virus membrane fusion

Katherine N. Liu and Steven G. Boxer

Supplementary Methods

Flow cell and glass coverslip preparation. Polydimethylsiloxane (PDMS) flow cells were prepared and plasma bonded to glass coverslips, as previously described (1). Briefly, glass coverslips (24 x 40 mm, No 1.5, VWR International, Radnor, PA) were cleaned by heating in 1:7 diluted 7X detergent in DI for 30 min, then rinsed extensively in DI water for 4 hours. Glass surfaces were annealed by baking slides in a kiln at 400 ℃ for 4 hours. PDMS flow cells (with channel dimensions 2.5 mm x 13 mm x 70 μm) and cleaned coverslips were plasma cleaned for at least 2 min and bonded together.

Surface functionalization. Glass slides were functionalized as previously described (2). Briefly, a 19:1 mixture of PLL-g-PEG (1 g/L) and PLL-g-PEG biotin (1 g/L) in HB buffer was incubated in flow cell for at least 30 min. Flow cells were rinsed with DI water and vesicle buffer, and stored overnight at 4˚C. The following day, neutrAvidin (1 g/L) was incubated for 15 min. After rinsing away excess neutrAvidin with vesicle buffer, biotin-DNA (178 μM, sequence A – see Table S1 for sequences) was incubated for 20 min. The flow cell was thoroughly rinsed with vesicle buffer to remove excess biotin-DNA.

Additional microscopy information. Sulforhodamine B images were obtained using a Texas Red filter cube (ex = 562/40 nm, bs = 593 nm, em = 624/40 nm) and additional excitation (560/55 nm) and emission (645/75 nm) filters. All images and video micrographs were captured with a frame rate of 288 ms/frame.

Viral labeling. IAV was labeled with TR-DHPE using methods previously described (1, 2). Briefly, TR-DHPE (0.75 g/L in ethanol) was mixed with HB buffer in a 1:40 ratio. 18 μL of IAV (2 mg/mL) was mixed with 72 μL of TR-DHPE/HB buffer solution and incubated for 2 hours at room temperature while rocking to incorporate fluorescently tagged lipids into IAV envelope. To separate unincorporated dye from labeled virions, about 1.35 mL of HB buffer was added and virus was pelleted by centrifugation at 21,130 rcf for 1 hour. The pellet that contained labeled virions was resuspended in 100 μL of fresh HB buffer.

Supported lipid bilayer (SLB) formation. SLBs were formed through vesicle fusion; 7 μL of vesicles (67.9% POPC, 20 % DOPE, 10% CH, 2% GD1a, and 0.1% OG-DHPE, conc. 0.56 mM) were added to a flow cell and incubated for 20-30 min to allow for SLB formation. Flow cells were subsequently rinsed at 1000 μL/min with at least 1 mL of DI water and 2 mL of vesicle buffer.

Table S1. DNA-lipid sequences.

Name	DNA sequence (5'-3')	Location
A	Biotin-TTT TTT TTT TTT TTT TTT TTT TTT	Glass slide
A'	Lipid-AAA AAA AAA AAA AAA AAA AAA AAA	Influenza envelope
B	Lipid-CCC CCC CCC CCC CCC CCC CCC CCC CCC CCC CCC CCC CCC CCC CCC CCC CCC CCC CCC CCC CCC CCC CCC CCC CCC TCG ACA CGG AAA TGT TGA ATA CTA	Influenza envelope
B'	Lipid-TAG TAT TCA ACA TTT CCG TGT CGA	Target vesicle (only vesicles with 10 mol% CH)
X	Lipid-TGC GGA TAA CAA TTT CAC ACA GGA-AF546	Vesicles (for DNA-lipid quantification)

Supplementary Results

Quantification of DNA-lipid incorporation in vesicles. The DNA-lipid incorporation into vesicles (67.9% POPC, 20% DOPE, 10% cholesterol, 2% GD1a, 0.1% OG-DHPE), was quantified by using an AlexaFluor-546 (AF546) labeled DNA-lipid (Sequence X, Table S1). The number of DNA-lipids in each vesicle was measured by quantitative fluorescence imaging, which is described in detail in previous studies (1, 3). Briefly, the average fluorescence intensity of one AF546 DNA-lipid was determined by single step photobleaching. AF546-labeled DNA-lipids were incorporated into vesicles, then vesicles were non-specifically bound to a glass slide in a PDMS microfluidic flow cell. After the flow cell was thoroughly rinsed, vesicles were imaged in the AF546 and OG-DHPE channels. The number of DNA-lipids in each vesicle was calculated by dividing the overall AF546 intensity by the average fluorescence intensity of one AF546 DNA-lipid.

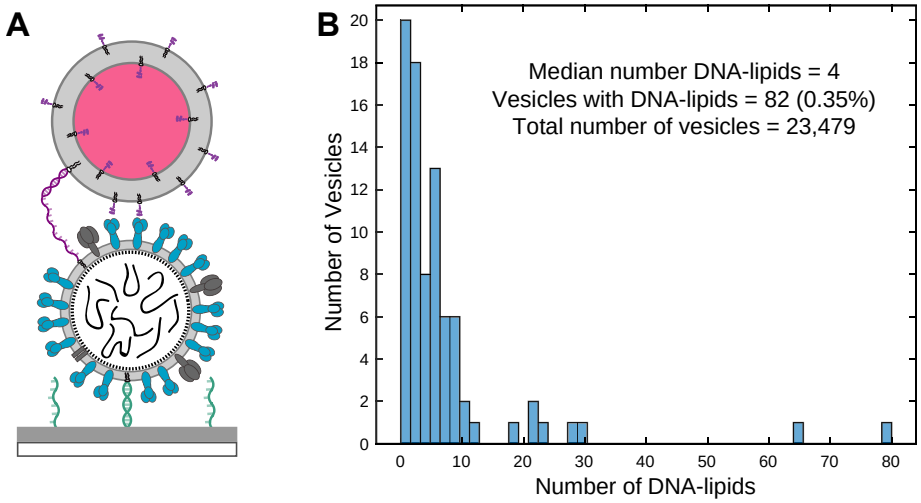

Figure S1. Distribution of DNA-lipids in 10% CH vesicles that contained at least one DNA-lipid.
A) Schematic of content mixing assay for vesicles containing 10 mol% CH, where in addition to GD1a, vesicles display DNA-lipids (purple, sequence B', Table S1), which hybridize to complementary DNA-lipids in IAV (sequence B). DNA-lipids were also used to tether IAV to vesicles in content mixing experiments that involved antibodies. B) Most vesicles did not display any DNA-lipids; the average number of DNA-lipids incorporated was 0.25/vesicle. Of the vesicles that displayed at least one DNA-lipid, the median number of DNA-lipids incorporated was 4. Total vesicles analyzed = 23,479.

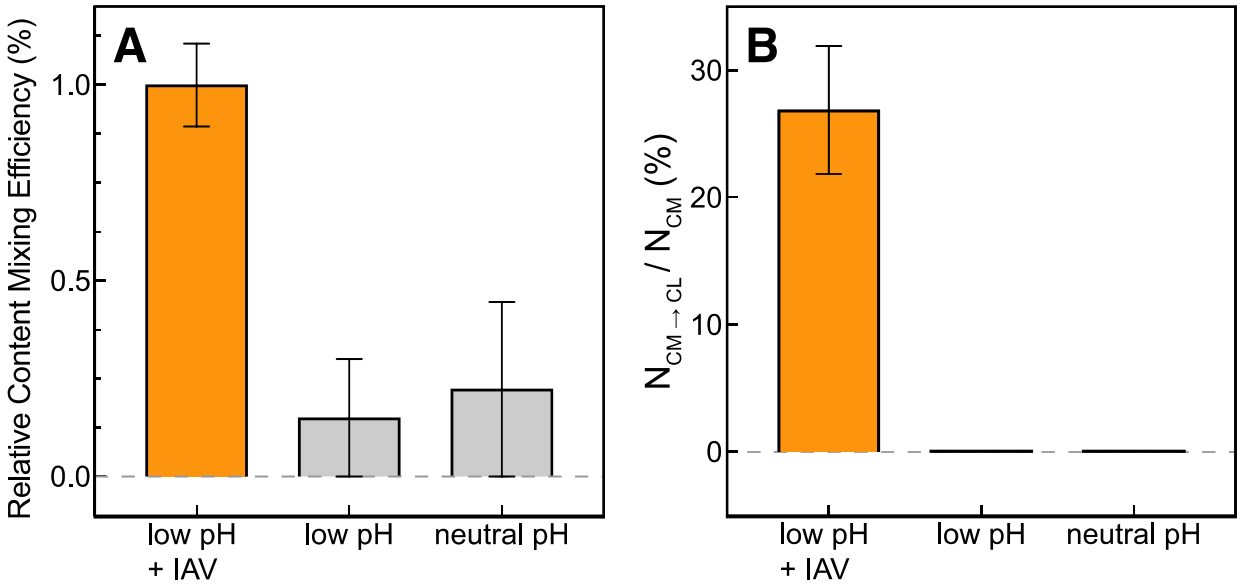

Figure S2. Content vesicle dequenching only occurs at pH 5.1 in the presence of influenza A virus.

In microfluidic flow cells, glass slides were functionalized as described in SI methods. For negative control experiments (gray), content-labeled vesicles (70% POPC, 20% DOPE, 10% CH) displayed DNA-lipids (sequence A') for surface tethering. Values represent the efficiency ± bootstrap resampling error. A) In the absence of IAV, there are a few content mixing events detected, but the number falls within error of the scripts used for analysis. The content mixing efficiency at low pH for IAV-bound vesicles is normalized to 1. B) In the absence of IAV, there are no content mixing events followed by content loss.

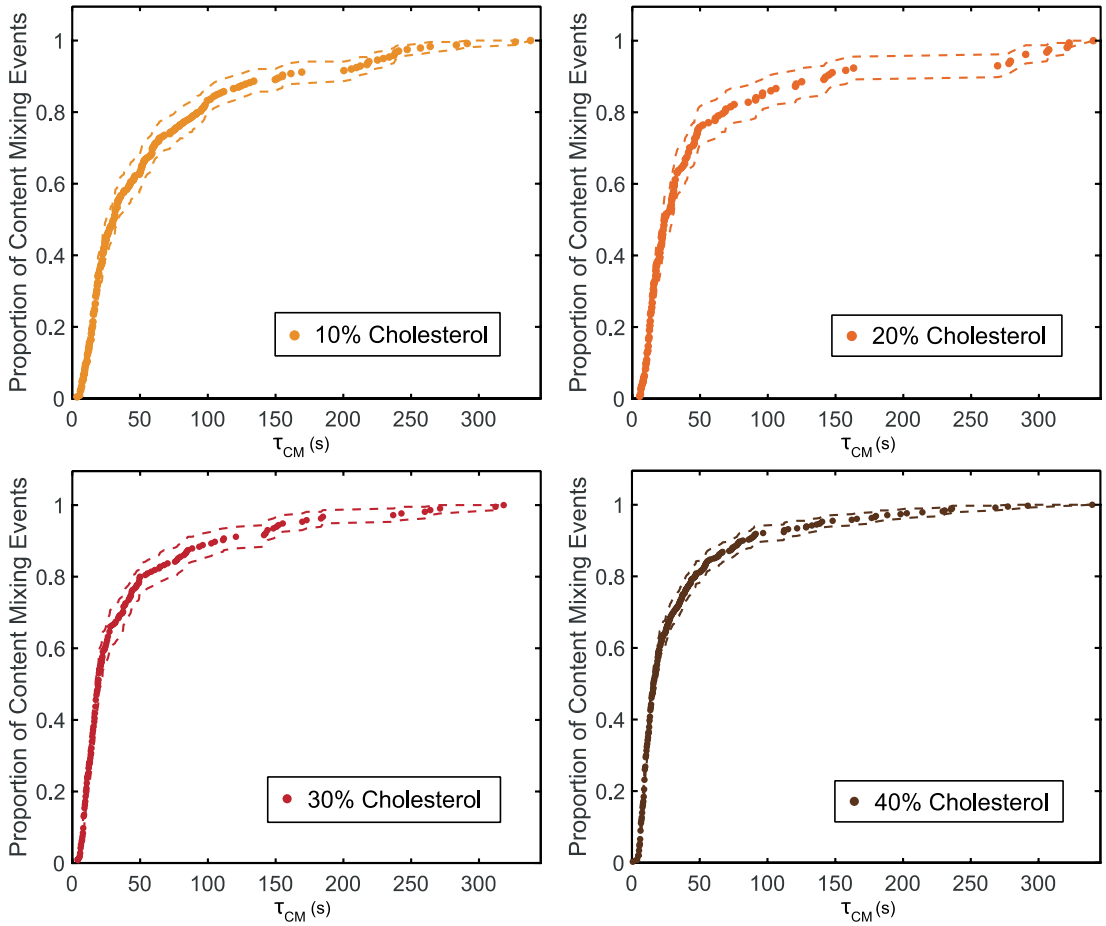

Figure S3. Individual CDFs for IAV content mixing to target vesicles with varying cholesterol compositions (merged in Fig. 3).

As in Fig. 3, wait times from pH drop to content mixing (τ_{CM}) for individual content mixing events are plotted as CDFs. Dashed lines represent bootstrap resampling error (95% confidence intervals). As the mol fraction of cholesterol (CH) in target vesicles increases, the efficiency also increases ~3.5-fold: 238/5250 for 10% CH, 157/2458 for 20% CH, 215/2153 for 30% CH, and 380/2411 for 40% CH. The total number of vesicles analyzed is proportional to the number of individual experiments executed, and not due to inherent differences in binding behavior. Kinetic data for each composition were compiled from at least four different independent viral preparations.

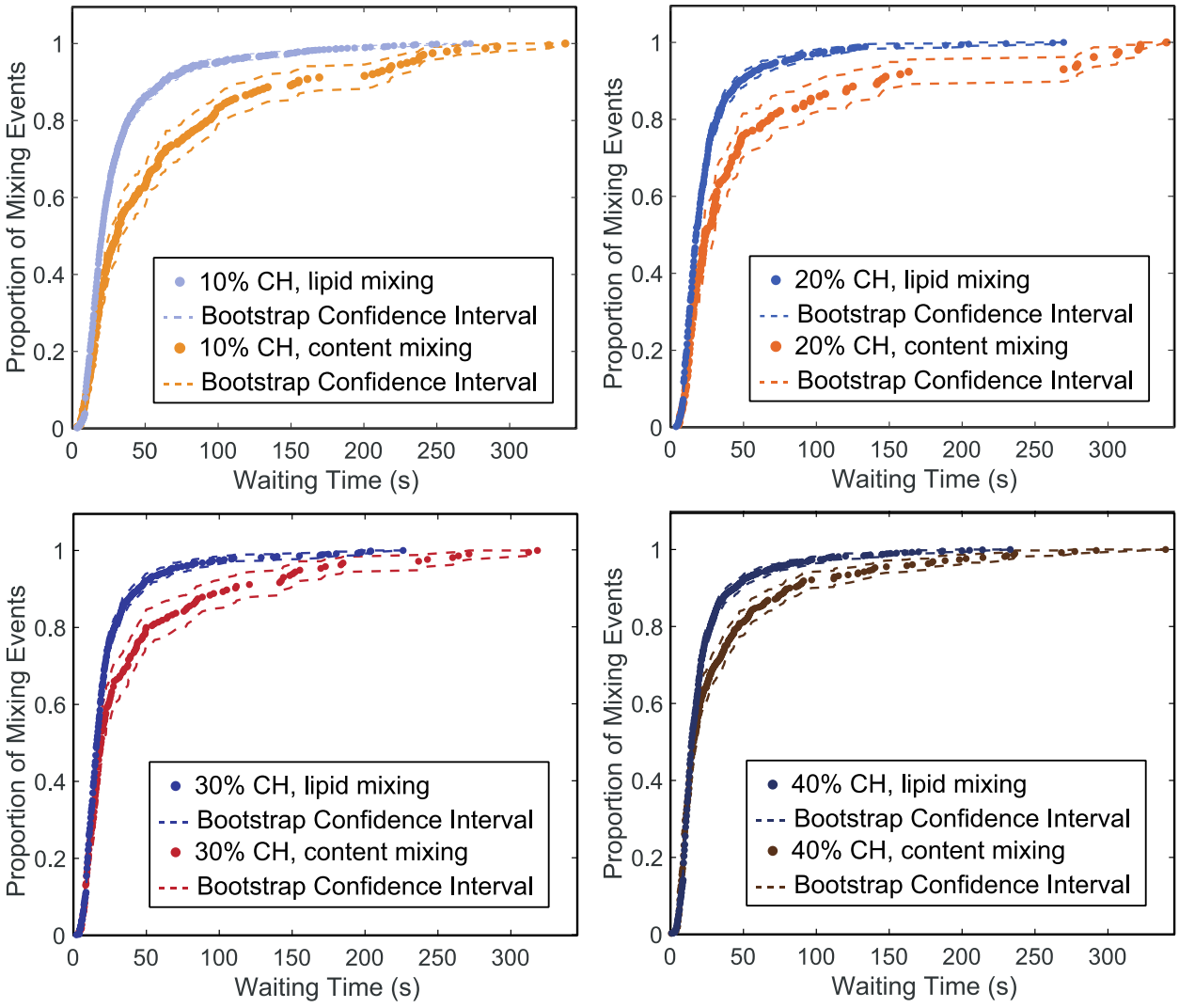

Figure S4. Comparison between lipid and content mixing rates for various target membrane compositions.

Target vesicles were tethered to IAV through GD1a. Content-labeled vesicles composed of 10% CH and all lipid-labeled vesicles were tethered through GD1a and DNA-lipid hybridization. Wait times from pH drop to lipid or content mixing for individual fusion events are plotted as CDFs. Lipid mixing traces were reproduced from reference (2) with permission. For all target vesicle compositions, content mixing is a slower process than lipid mixing (within bootstrap resampling error, 95% confidence intervals, dashed lines).

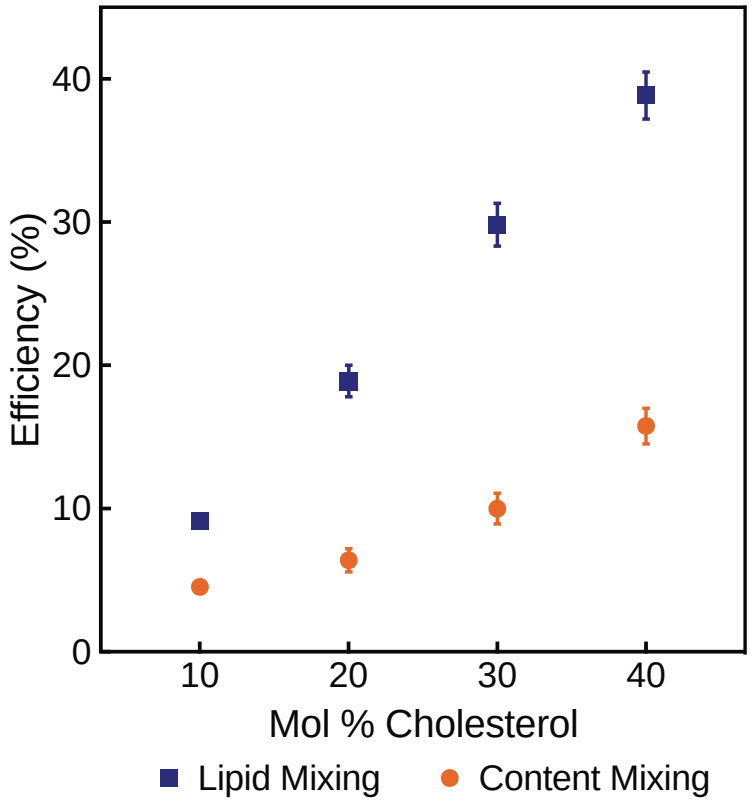

Figure S5. Comparison between lipid and content mixing efficiencies for various target membrane compositions.
Target vesicles were tethered to IAV through GD1a. Content-labeled vesicles composed of 10% CH and all lipid-labeled vesicles were tethered through GD1a and DNA-lipid hybridization. For all compositions, the lipid mixing efficiency was roughly two to three times greater than the corresponding content mixing efficiency, which suggests that a significant fraction of lipid mixing events do not result in full fusion. Points represent the efficiency value ± bootstrap resampling error; lipid and content mixing data were collected in separate experiments.

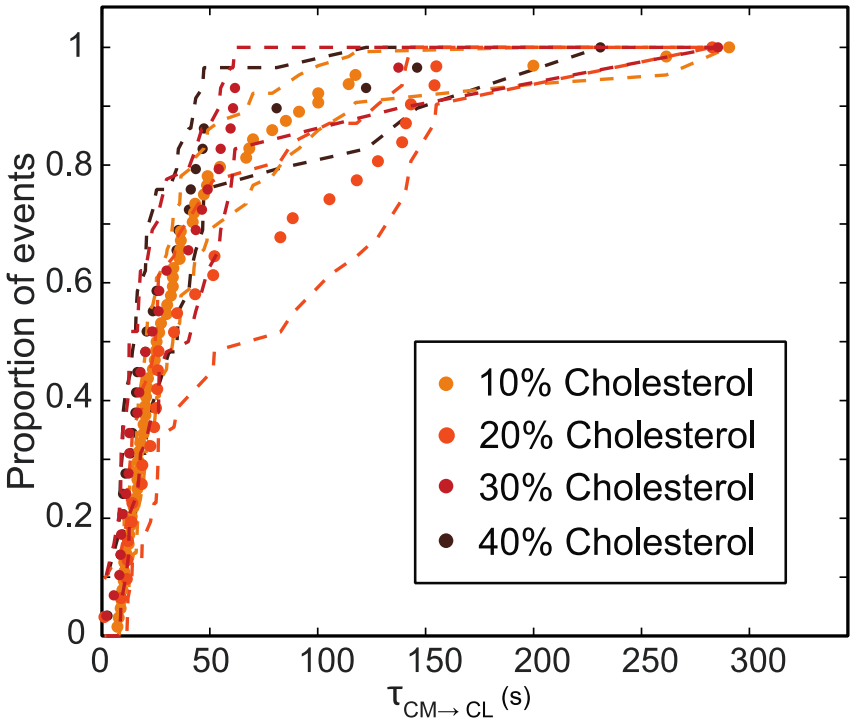

Figure S6. Comparison of intervals from content mixing to content loss for vesicles containing various amounts of CH.

$\tau_{CM \rightarrow CL}$ values for individual events are plotted as CDFs. $N_{CM \rightarrow CL}$ values for vesicles that contained a high fraction of CH were too low to observe any significant difference between compositions. Dashed lines represent bootstrap resampling error with 95% confidence intervals. $N_{CM \rightarrow CL}$ = 64 (10% CH), 31 (20% CH), 29 (30% CH), 29 (40% CH).

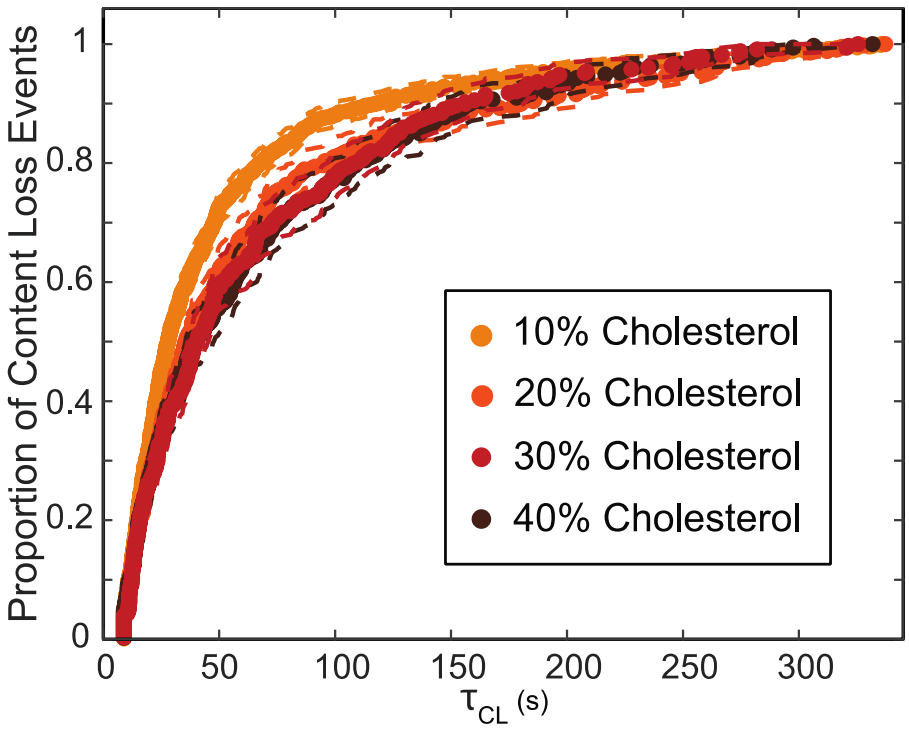

Figure S7. The rate of content loss events is not affected by target membrane cholesterol. Wait times from pH drop to content loss (τ_{CL}) for individual events are plotted as CDFs. For all target membrane compositions tested, the rate of content loss is the same within bootstrap resampling error (95% confidence intervals, dashed lines). As CH in target vesicles increases, there is no significant difference in the fraction of vesicles that undergo content loss: 724/5250 for 10% CH, 427/2458 for 20% CH, 328/2153 for 30% CH, and 333/2411 for 40% CH.

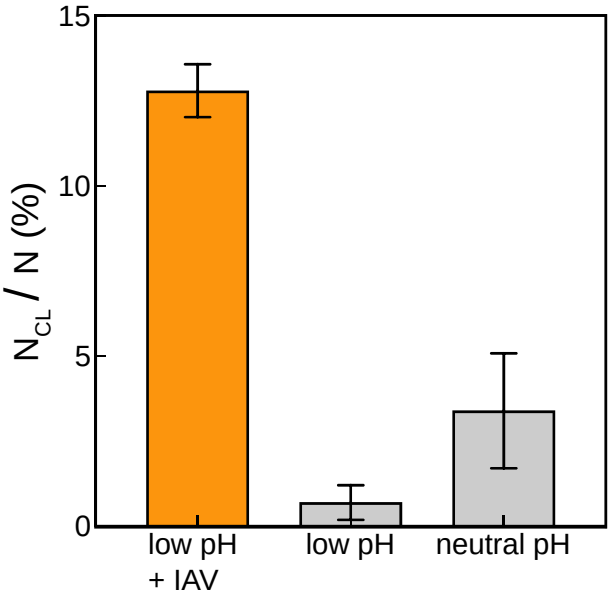

Figure S8. There are significantly more content loss events at low pH when vesicles are tethered to IAV.

In microfluidic flow cells, glass slides were functionalized as described in SI methods. For negative control experiments (gray), content-labeled vesicles (70% POPC, 20% DOPE, 10% CH) displayed DNA-lipids (sequence A') for surface tethering. Values represent the frequency of content loss ± bootstrap resampling error**.** Due to the baseline of content loss events that take place when flow cells are exchanged with neutral pH buffer, all experiments were rinsed with a standardized amount of buffer.

Single-virus binding assay to test for antibody coverage. The design for this single-virus binding assay was based on previous studies (4, 5). 4 µL of TR-DHPE labeled IAV (2 mg/mL) were incubated with 1 µL of solutions of monoclonal antibodies (various concentrations, diluted in HB buffer) for 2 hours at room temperature (22˚C), then samples were kept on ice. In a flow cell, 1 µL of antibody-bound virions was introduced to a GD1a-displaying SLB and allowed to bind for 60 seconds. Unbound virions were rinsed away at 600 µL/min using vesicle buffer, and the resulting number of bound virions for each FOV was quantified through spot analysis of fluorescence micrographs using MATLAB scripts.

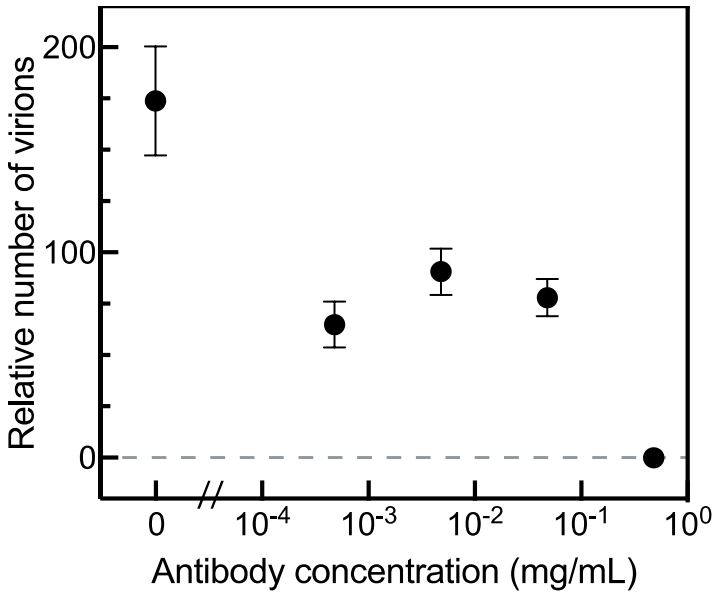

Figure S9. Antibodies decrease IAV binding to a supported lipid bilayer displaying GD1a. Points represent the average number of virions bound/FOV ± standard deviation. At least 35 images were taken for each concentration of antibodies.

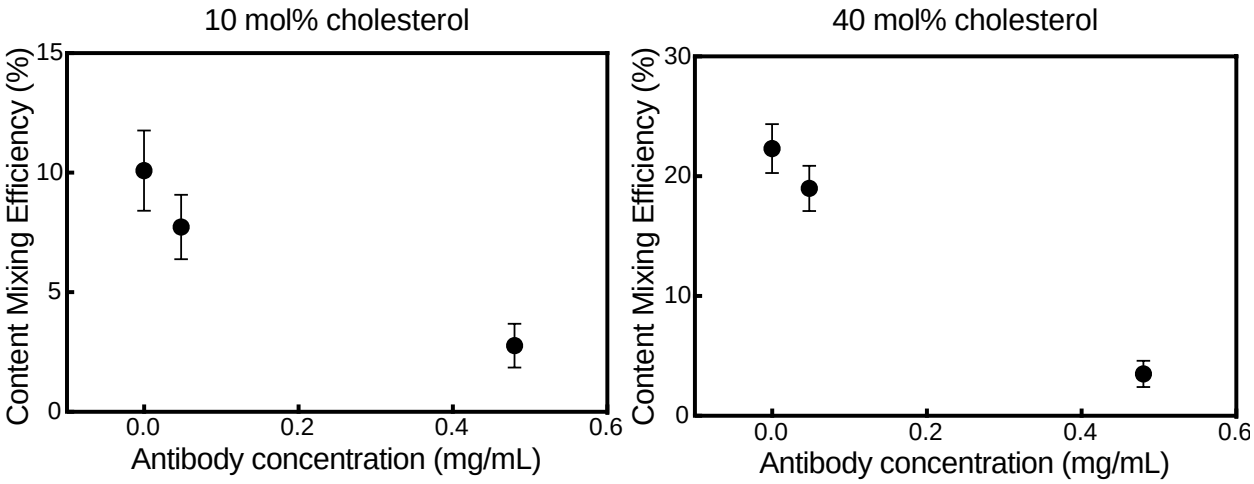

Figure S10. Antibodies decrease the efficiency of content mixing to target vesicles containing 10 and 40 mol% cholesterol.

Influenza A virions were incubated with various concentrations of monoclonal antibodies. Content-labeled vesicles composed of 10 and 40 mol% cholesterol were tethered to virions through DNA-lipid hybridization, and the pH was lowered to trigger content mixing and content loss. For both target membrane compositions, the addition of antibodies to IAV decreased the content mixing efficiency. Each data point represents at least 900 vesicles analyzed ± bootstrap resampling error.

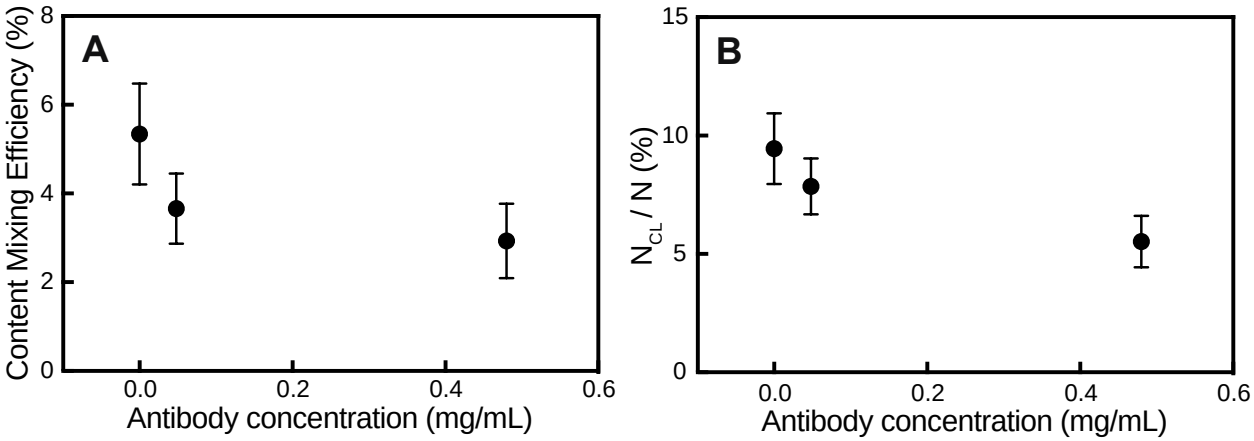

Figure S11. Antibodies decrease the fraction of IAV content mixing and content loss events in the absence of GD1a.

Influenza A virions were incubated with various concentrations of monoclonal antibodies. Content-labeled vesicles (40% CH, 20% DOPE, 40% POPC) that did not contain GD1a were tethered to IAV through DNA-lipid hybridization. When the pH was lowered to trigger A) content mixing and B) content loss, we observed that in the absence of HA-GD1a interaction, antibodies also decrease the frequency of both content mixing and content loss events ± bootstrap resampling error. Each data point reflects at least 1200 vesicles analyzed.

References

1. Rawle, R.J., S.G. Boxer, and P.M. Kasson. 2016. Disentangling Viral Membrane Fusion from Receptor Binding Using Synthetic DNA-Lipid Conjugates. Biophys. J. 111: 123–131.
2. Liu, K.N., and S.G. Boxer. 2020. Target Membrane Cholesterol Modulates Single Influenza Virus Membrane Fusion Efficiency but Not Rate. Biophys. J. 118: 2426–2433.
3. Van Lengerich, B., R.J. Rawle, P.M. Bendix, and S.G. Boxer. 2013. Individual vesicle fusion events mediated by lipid-anchored DNA. Biophys. J. 105: 409–419.
4. Delaveris, C.S., E.R. Webster, S.M. Banik, S.G. Boxer, and C.R. Bertozzi. 2020. Membrane-tethered mucin-like polypeptides sterically inhibit binding and slow fusion kinetics of influenza A virus. Proc. Natl. Acad. Sci. U. S. A. 117: 12643–12650.
5. Goronzy, I.N., R.J. Rawle, S.G. Boxer, and P.M. Kasson. 2018. Cholesterol enhances influenza binding avidity by controlling nanoscale receptor clustering. Chem. Sci. 9: 2340–2347.